JOURNAL OF PETROLOGY | VOLUME 42 | NUMBER 11 | PAGES 1995–2013 | 2001

P–T–t Evolution of Ultrahigh-Temperature Granulites from the Saxon Granulite Massif, Germany. Part I: Petrology

JOCHEN RÖTZLER[1]* AND ROLF L. ROMER[2]

[1]INSTITUT FÜR GEOWISSENSCHAFTEN, UNIVERSITÄT POTSDAM, POSTFACH 60 15 53, 14415 POTSDAM, GERMANY
[2]GEOFORSCHUNGSZENTRUM POTSDAM, TELEGRAFENBERG, 14473 POTSDAM, GERMANY

RECEIVED JANUARY 28, 2000; REVISED TYPESCRIPT ACCEPTED APRIL 16, 2001

The granulites of the Saxon Granulite Massif equilibrated at high pressure and ultrahigh temperature and were exhumed in large part under near-isothermal decompression. This raises the question of whether P–T–t *data on the peak metamorphism may still be retrieved with confidence. Felsic and mafic granulites with geochronologically useful major and accessory phases have provided a basis to relate* P–T *estimates with isotopic ages presented in a companion paper. The assemblage garnet + clinopyroxene in mafic granulite records peak temperatures of 1010–1060°C, consistent with minimum estimates of around 967°C and 22·3 kbar obtained from the assemblage garnet + kyanite + ternary feldspar + quartz in felsic granulite. Multiple partial overprint of these assemblages reflects a clockwise* P–T *evolution. Garnet and kyanite in the felsic granulite were successively overgrown by plagioclase, spinel + plagioclase, sapphirine + plagioclase, and biotite + plagioclase. Most of this overprinting occurred within the stability field of sillimanite. Garnet + clinopyroxene in the mafic granulite were replaced by clinopyroxene + amphibole + plagioclase + magnetite. The high* P–T *conditions and the absence of thermal relaxation features in these granulites require a short-lived metamorphism with rapid exhumation. The ages of peak metamorphism (342 Ma) and shallow-level granitoid intrusions (333 Ma) constrain the time span for the exhumation of the Saxon granulites to ~ 9 my.*

KEY WORDS: *ultrahigh-temperature metamorphism; granulite; thermobarometry; exhumation; Saxon Granulite Massif*

INTRODUCTION

The Variscan high-pressure metamorphism in the Bohemian Massif reflects separate, pre- and syn-collisional subduction events in Silurian–Devonian and Devonian–Carboniferous times, with both having produced blueschist–eclogite to granulite facies metamorphic complexes. This dualism, which was first described by Pin & Vielzeuf (1983) from various parts of the European Variscides, has been verified by recent work (e.g. Kryza *et al.*, 1996; Rötzler *et al.*, 1999). The thermotectonic modelling of the Variscan geodynamic evolution depends on the *P–T* information that is preserved in exhumed high-pressure and high-temperature rocks and on whether it still records peak conditions. In this respect, the various occurrences of ultrahigh-temperature granulite within the Bohemian Massif are particularly problematic, as they underwent near-isothermal decompression, which caused minor (Snieznik granulites; see Kryza *et al.*, 1996) to intense (Moldanubian granulites; see Petrakakis, 1997) post-peak overprint. In these rocks, the multiple partial overprinting at ultrahigh to high temperatures also makes it difficult to relate isotopic ages to mineral assemblages and *P–T* data. The problem can be solved only if petrology and geochronology are jointly investigated. In this study, we use mineral assemblages and compositions of selected rock types to constrain a *P–T* path for the Saxon Granulite Complex. In a second paper (Romer & Rötzler, 2001), we date various minerals from the same rocks by the U–Pb method and relate their ages to *P–T* estimates.

*Corresponding author. Telephone: +49-331-977-5078. Fax: +49-331-977-5060. E-mail: jroetzler@geo.uni-potsdam.de

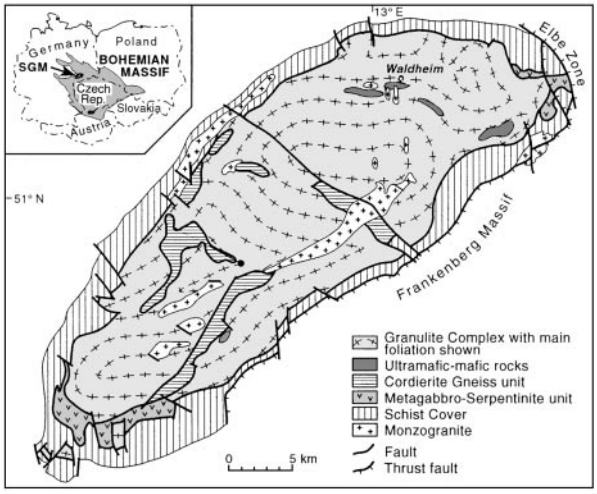

Fig. 1. Geological map of the Saxon Granulite Massif.

GEOLOGICAL SETTING

The Saxon Granulite Complex and structurally overlying units of lower metamorphic grade constitute the Saxon Granulite Massif (SGM), a NE–SW-trending dome structure within the Variscan basement at the northwestern margin of the Bohemian Massif. This dome plunges to the SE beneath the nappe complex of the Frankenberg Massif, which was emplaced during a short period of time between the cooling in the underlying envelope of the Granulite Complex at 333 Ma (Werner & Reich, 1997) and the sealing of the nappe contacts by red beds dated to ~330 Ma (Gaitzsch, 1998). The northeastern boundary of the SGM is covered by low-grade to very low grade Palaeozoic rocks of the Elbe Zone, which were overthrust at ~300 Ma (Rauche, 1994). Along its northwestern and southwestern flanks, the SGM is bounded by post-orogenic red beds and acid volcanic rocks (Fig. 1).

The internal structure of the SGM shows an excision of large parts of the metamorphic zonation from the Granulite Complex to the overlying units, but also within the latter. The Granulite Complex is overlain for the most part by a low-pressure unit referred to as the Schist Cover. This unit is formed by a tectonically condensed right-way-up sequence, ~3500 m thick, of Upper Proterozoic to Upper Devonian shelf deposits with minor metavolcanic intercalations. The metamorphic grade in the Schist Cover increases across concentric, closely spaced isograds up to high-grade conditions at the contact with the granulites (Rötzler, 1992). The Granulite Complex and Schist Cover are separated by a fault zone that accommodates relics of various dismembered rock units. Among these relics are high-grade metapelites (Cordierite Gneiss unit), oceanic meta-igneous rocks (Metagabbro–Serpentinite unit), and orthogneiss. Age data derived from detrital zircon and from zircon overgrowths support a Cambrian sedimentary age of the Cordierite Gneiss unit (Vavra & Reinhardt, 1997). This unit shows a clockwise P–T path, with medium-pressure conditions followed by pressure release and heating to a stage that falls on the retrograde path of the Granulite Complex (Rötzler, 1992).

The surface exposure of the Granulite Complex consists mainly of felsic garnet–kyanite granulite. Felsic–mafic compositional layering occurs in some areas, but even there, felsic granulite prevails over centimetre- to metre-thick interlayers of garnet–orthopyroxene, garnet–two-pyroxene or garnet–clinopyroxene granulite. This layering (S_1) is mostly parallel to the granulite facies mylonitic main foliation (S_2), but was locally deformed by isoclinal intrafolial folds within S_2. Decametre-thick lenses of mafic granulite occur only in a few places. On geochemical and isotopic criteria, the Granulite Complex consists almost exclusively of meta-igneous rocks (Werner, 1987; Rötzler, 1992; von Quadt, 1993; Hagen, 1994). Minor lithologies, such as quartz-rich or boron silicate-bearing felsic granulites and garnet–clinopyroxene granulites of supposed calc-silicate nature, were interpreted as metasediments (Werner, 1987; Grew, 1989). However, a sedimentary origin of these rocks is challenged, at least in part, by oxygen isotope data (Hagen, 1994). Largely serpentinized ultramafic–mafic rocks, up to several square kilometres in extent, form sheet-like bodies parallel to the main foliation of the granulites. Prograde or peak-metamorphic partial melting or intrusion are nowhere in evidence in the Granulite Complex, as opposed to local retrograde partial melting, which occurred in response to decompression and hydration.

Earlier isotopic dating of the granulites provided possible protolith ages and a number of ages with controversial significance for the metamorphic evolution. Whole-rock and mineral isochron Sm–Nd ages of 470 Ma, 380 Ma and 346–335 Ma were interpreted to represent the protolith age and two subsequent high-pressure metamorphic events, respectively. A single P–T loop or polymetamorphism were thus considered possible (von Quadt, 1993). From apparent monazite ages, Baumann *et al.* (1997) concluded that the granulites cooled through the monazite closing temperature at ~315 Ma. This, however, is difficult to reconcile with K–Ar mica ages, which indicate cooling of the Schist Cover as early as 333 Ma (Werner & Reich, 1997), and with the erosion of the Granulite Complex at ~310 Ma, as proved by the appearance of granulite debris in post-orogenic red beds. Because of evidence in the Schist Cover for post-metamorphic fluid-induced rejuvenation of monazite, Vavra *et al.* (1998) suspected a similar alteration of the granulite monazites, making it probable that the Granulite Complex cooled before 315 Ma. Accordingly, they interpret zircon U–Pb ion-probe data, covering the

range 355–320 Ma, as reflecting metamorphic zircon growth at 355 Ma or earlier, followed by fluid-induced zircon alteration at 320 Ma or later. Zircon ages within this range are assigned no geological meaning. Kröner *et al.* (1998) analysed zircon from felsic granulites by ion probe, by Pb evaporation and by conventional dissolution techniques, and reported the following characteristics: (1) Precambrian inheritance; (2) 485–470-my-old cores, interpreted as dating the protoliths; (3) zircon growth and overgrowth at ~340 Ma, thought to reflect near-peak granulite facies conditions. The last feature is in agreement with zircon U–Pb ages presented by von Quadt (1993). No older metamorphic zircon was found, and apparent ion-probe and evaporation ages between 470 and 340 Ma were taken as geologically meaningless mixed ages. Conventional zircon U–Pb data were considered as an ambiguous indication of igneous crystallization at ~405 Ma. Zircon U–Pb ion-probe analyses on various monzogranite bodies within the Granulite Complex and the marginal mylonite zone revealed a uniform intrusion age of 333 Ma (Nasdala *et al.*, 1996; Kröner *et al.*, 1998).

Evidence in the Granulite Complex of ultrahigh temperatures at pressures of 20 kbar (Rötzler *et al.*, 1994; Hagen *et al.*, 1995) implies that the pressure release from 12 kbar, proposed by Grew (1986) and Rötzler (1992), represents only the late section of a protracted near-isothermal decompression path. In an attempt to resolve this evolution, we looked for mineral assemblages that would allow pressure, temperature and time of peak and post-peak equilibration to be defined. The samples were to contain geochronologically useful minerals, including major and accessory phases, which can be related with confidence to mineral assemblages and P–T estimates. Moreover, the samples were selected to be least retrograde for analysing U–Pb, but visibly hydrated for extracting Rb–Sr biotite data. Three rock samples from Waldheim were found to meet these requirements best. Of these, two (G97-1 and G97-2) are from a railway cut at Pfaffenberg hill, whereas the third (G97-3) was collected NE of Waldheim station. The sample localities (using German national grid reference numbers as given in the 1:25 000 scale map 4944, Waldheim) are as follows: G97-1: 5659910, 4571330 (Pfaffenberg hill); G97-2: 5659675, 4571300 (Pfaffenberg hill); G97-3: 5660625, 4571250 (Waldheim station). The field relations of all three samples agree with those described above for felsic and mafic granulites.

PETROGRAPHY AND REACTION TEXTURES

Sapphirine-bearing granulite (G97-1)

This rock represents an interlayer a few metres thick in felsic granulite that is exposed as loose blocks. It is readily distinguished at hand-specimen scale from the country rock by a higher abundance of garnet. The sapphirine-bearing granulite is enriched in Fe, Mg, Al and Ti but depleted in Si compared with the dominant type of felsic granulite. This particular rock is a new occurrence of sapphirine, differing from the known localities for this mineral in the SGM (Grew, 1986, 1989) by the absence of boron silicate phases.

The sapphirine-bearing granulite is modally abundant in garnet (22%), quartz (34%), mesoperthite (27%) and plagioclase (14%). The protomylonitic texture is formed by a fine-grained quartzo-feldspathic matrix with accessory rutile, apatite, pyrrhotite, pyrite, graphite, zircon and monazite, and by anhedral megacrysts of garnet, less commonly of kyanite and mesoperthite. Impersistent quartz ribbons define a clear foliation. Plagioclase is concentrated around garnet and kyanite, partly in association with other reaction products of these minerals. The mineral inclusions in garnet comprise biotite, kyanite, quartz, plagioclase, mesoperthite, rutile, pyrrhotite and zircon.

A succession of mineral reactions is evident from multiple overgrowths on garnet and kyanite, with kyanite being more strongly resorbed than garnet. Most kyanite crystals have spinel–plagioclase coronas that also contain corundum in places. Garnet is only locally overgrown by spinel–plagioclase aggregates. The spinel–plagioclase coronas and kyanite are commonly separated by sapphirine–plagioclase symplectite (Fig. 2a). A similar texture is found at garnet rims. There, sapphirine–plagioclase symplectite grows from outer spinel–plagioclase aggregates into the garnet core (Fig. 2b and c). The most prominent results of these reactions are pseudomorphs after kyanite and recrystallized atoll-like garnet rims filled with sapphirine–plagioclase symplectite (Fig. 2d). Spinel, corundum and sapphirine are shielded from the matrix by plagioclase and are not observed in contact with quartz. Part of the kyanite, including relics within the above reaction textures, has been transformed to sillimanite. Although mutual contacts of garnet and kyanite are rarely preserved, it may be concluded from the reaction textures that kyanite was partly originally armoured by garnet. This textural relation is commonly observed in felsic granulites from the SGM. The overgrowth on garnet and kyanite, partly represented by simple plagioclase coronas and partly by multiple coronas of outer plagioclase and the above-described inner reaction textures, thus suggests that garnet and kyanite first underwent GASP back reaction, then the reaction Grt + Ky = Spl + Pl ± Crn, and finally the reaction Grt + Ky + Spl = Spr + Pl. The latter two reactions are likely to have been active within the stability field of sillimanite, as the reaction products are locally intimately intergrown with sillimanite.

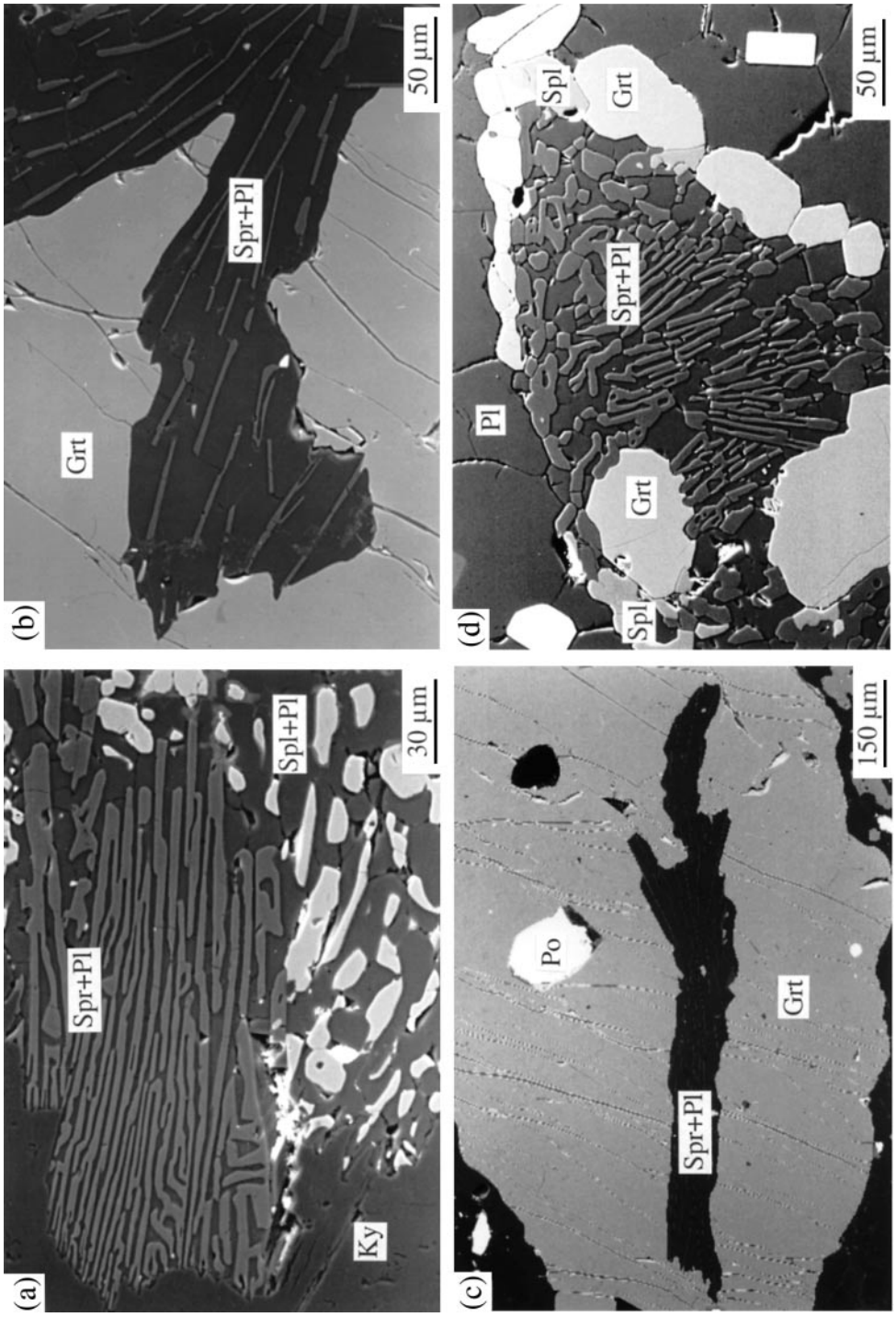
(a)
Spr+Pl
Spl+Pl
Ky
30 μm
(b)
Grt
Spr+Pl
50 μm
(c)
Po
Grt
Spr+Pl
150 μm
(d)
Spl
Grt
Pl
Spr+Pl
Grt
Spl
50 μm

Fig. 2 (a–d).

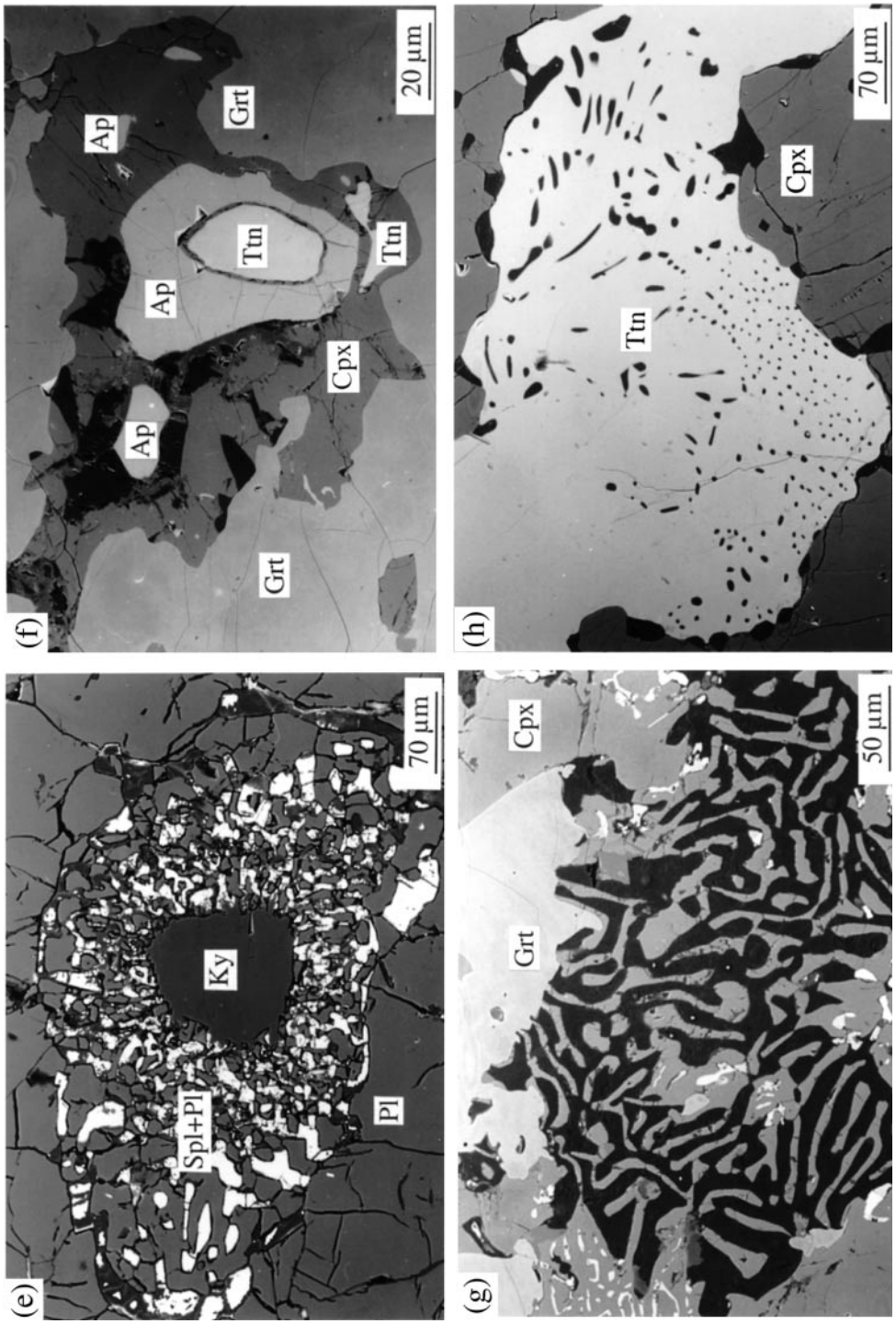

Fig. 2 (a). Back-scattered electron images of metamorphic textures. (a–d) Sapphirine-bearing granulite (G97-1): (a) outer spinel–plagioclase corona and inner sapphirine–plagioclase symplectite on kyanite; (b) sapphirine–plagioclase symplectite penetrating into a garnet megacryst; (c) sapphirine–plagioclase symplectite included in garnet, with the same texture and composition as the symplectite outside of the garnet; (d) partially recrystallized atoll-like relics of a garnet megacryst, largely replaced by sapphirine–plagioclase symplectite. The garnet is penetrated by spinel and sapphirine, and the entire texture is surrounded by a moat of plagioclase. (e) Retrogressed felsic granulite (G97-2): kyanite relic overgrown by a spinel–plagioclase corona and enveloped in outer plagioclase. (f–h) Garnet–clinopyroxene granulite (G97-3): (f) inclusions of clinopyroxene (Cpx_1), apatite and titanite in garnet; (g) replacement of garnet and matrix clinopyroxene (Cpx_2) by symplectite of clinopyroxene (Cpx_3), pargasite, plagioclase and magnetite; (h) plagioclase exsolution blebs in titanite.

These decompression mineral assemblages are locally cut or overgrown by minor retrograde biotite that is also found at garnet rims and within fractures in garnet. Overgrowths of chlorite on garnet and biotite, partly in association with rutile needles or titanite, and growth of muscovite on garnet, sillimanite or feldspar reflect the late stage. The metamorphic stages can be summarized by the following assemblages:

(1) Grt–Ky–Bt–Afs–Pl–Qtz–Rt–Ap–Gr–Po–Zrn–Mnz (pre-peak stage);

(2) Grt–Ky–hypersolvus ternary feldspar–Qtz–Rt–Ap–Gr–Po–Zrn–Mnz (peak stage);

(3) Grt–Sil–Spl–Crn–Spr–Afs–Pl–Rt–Ap–Gr–Po–Py (decompression stage);

(4) Grt–Sil–Bt–Kfs–Pl–Qtz (biotite stage);

(5) Chl–Ms–Pl–Qtz–Rt–Ttn (late stage).

Retrogressed felsic granulite (G97-2)

This rock formed by retrograde overprinting of the dominant type of felsic granulite. It has a modal composition of 38% quartz, 35% alkali feldspar, 19% plagioclase and 8% biotite. Garnet is largely replaced by clusters of biotite, which impart a patchy appearance to the light-coloured rock. Minor leucosome lenses are locally observed.

The fine-grained rock has a granoblastic inequigranular texture with lobate grain contacts. Quartz shows a continuous gradation in grain size up to porphyroblasts that parallel a weak foliation. Distinct feldspar recrystallization is evident from a loss of the lamellar exsolution texture in outer parts of perthite grains and from local transformation of these grains to microcline. Some strongly corroded relics of kyanite are mantled by an inner corona of spinel + plagioclase and outer coronitic plagioclase (Fig. 2e). As in less altered felsic granulite, this texture formed at the expense of garnet rims around kyanite. Most of the kyanite, however, is pseudomorphed by dense aggregates of prismatic sillimanite. Both reaction textures are locally intimately associated, suggesting a close temporal relationship between the transformation of kyanite to sillimanite and the spinel-forming reaction.

Red–brown or greenish biotite replaces garnet. Biotite also overgrows sillimanite, and both minerals are commonly surrounded by plagioclase. This reflects the biotite-forming reaction Grt + Sil + Kfs + H_2O = Bt + Pl + Qtz. Late alterations comprise the overgrowth of haematite and muscovite on feldspar and of chlorite on biotite. Hence, this retrogressed granulite shows a similar metamorphic evolution as the sapphirine-bearing granulite, although the early stages are less well preserved.

Garnet–clinopyroxene granulite (G97-3)

This lens of mafic granulite, up to 15 m thick, is concordant with the foliation in surrounding felsic granulite. It preserves peak-metamorphic domains consisting overwhelmingly of garnet and clinopyroxene. A layered fabric is defined by variations in the ratio of these minerals on a millimetre to centimetre scale, with clinopyroxene-rich layers prevailing over garnet-rich ones. Retrograde overprinting enhanced the heterogeneity in modal composition, producing major amounts of amphibole and muscovite in places.

The granoblastic texture of this fine- to medium-grained rock is formed by the peak assemblage garnet + clinopyroxene + titanite + apatite. Titanite and apatite are minor phases, which occur both free in the matrix and as inclusions in garnet (Fig. 2f). Clinopyroxene is subdivided into three textural types. Early clinopyroxene (Cpx_1) and spinel occur as inclusions in garnet, suggesting that garnet grew from these minerals and, probably, from plagioclase. Garnet and matrix clinopyroxene (Cpx_2) are partially replaced by symplectite made of late clinopyroxene (Cpx_3), amphibole, plagioclase and magnetite (Fig. 2g). This reflects the retrograde reaction Grt + Cpx_2 + H_2O = Cpx_3 + Am + Pl + Mag. Plagioclase is also present in traces within, and as fine rims on, clinopyroxene grains in the matrix. Vermicular blebs of plagioclase are found within titanite (Fig. 2h). Because most of the plagioclase is overgrown by muscovite, potassium must have entered the system during late-stage infiltration of an external fluid.

MINERAL CHEMISTRY

The sapphirine-bearing granulite (G97-1) and the garnet–clinopyroxene granulite (G97-3) were analysed at the GeoForschungsZentrum (GFZ) Potsdam using a Cameca SX50 electron microprobe with four wavelength-dispersive spectrometers. Operating conditions were 15 kV accelerating voltage and 20 nA sample current. Counting times of 10–20 s and beam diameters of 1–10 μm were applied, depending on element contents and volatile components. Natural and synthetic standards were used and the data were processed by the PAP routine. Representative mineral compositions are listed in Tables 1–5.

Garnet in the sapphirine-bearing granulite, where overgrown by spinel and sapphirine, is a fairly homogeneous pyrope–almandine solid solution with low grossular contents (52–41 mol % pyrope, 46–56 mol % almandine, 0–5 mol % grossular). Garnet rims and walls of garnet cracks adjacent to biotite or chlorite are less pyropic. The garnet rims show a drop in X_{Mg} [Mg/(Mg + Fe^{2+})] from 0·49–0·48 in contact with spinel or sapphirine, through 0·43–0·41 in contact with biotite, to 0·34 in contact with chlorite. However, garnet megacrysts not associated with spinel or sapphirine are strongly zoned, preserving two groups of relic Ca-rich cores. Of these, the first has 25 mol % grossular and a relatively low X_{Mg}

Table 1: Representative garnet compositions

Sample:	G97-1	G97-1	G97-1	G97-1	G97-1	G97-1	G97-3	G97-3	G97-3	G97-3	G97-3	G97-3
Analysis:	15A	35A	3-17B	20-22B	24-33B	40-46B	1	19	21	23	26	27
Position:	rim	rim	core	core	core	rim	rim	core	core	core	core	core
SiO_2	39·38	38·60	40·13	39·31	39·65	39·86	38·60	39·26	39·34	39·21	39·41	38·92
TiO_2	0·02	0·01	0·05	0·19	0·11	0·04	0·24	0·33	0·34	0·35	0·38	0·31
Al_2O_3	22·70	21·81	22·74	22·36	22·63	22·69	21·31	19·91	19·58	19·43	19·96	19·90
FeO^T	24·02	29·70	21·99	19·70	20·20	23·67	17·04	15·92	15·77	15·88	15·68	15·89
MnO	0·26	0·52	0·34	0·41	0·36	0·40	0·42	0·33	0·34	0·32	0·24	0·37
MgO	12·46	8·42	13·33	8·19	10·72	12·48	4·36	4·86	4·80	4·88	4·82	4·81
CaO	0·84	1·28	1·34	9·51	6·19	0·73	17·55	19·41	19·57	19·10	19·49	19·43
Total	99·68	100·34	99·92	99·67	99·86	99·87	99·52	100·02	99·74	99·17	99·98	99·63
Cations per 24 oxygens												
Si	5·96	5·97	6·00	5·98	5·98	6·00	5·95	5·99	6·03	6·04	6·01	5·98
Ti	0·00	0·00	0·01	0·02	0·01	0·01	0·03	0·04	0·04	0·04	0·05	0·04
Al	4·05	3·98	4·00	4·02	4·02	4·02	3·88	3·59	3·53	3·52	3·59	3·60
Fe^{3+}	0·00	0·05	0·00	0·00	0·00	0·00	0·14	0·39	0·40	0·40	0·35	0·38
Fe^{2+}	3·04	3·80	2·75	2·51	2·55	2·98	2·05	1·65	1·62	1·64	1·65	1·66
Mn	0·04	0·07	0·05	0·06	0·05	0·05	0·06	0·05	0·05	0·05	0·03	0·05
Mg	2·81	1·94	2·97	1·86	2·41	2·80	1·00	1·11	1·10	1·12	1·10	1·10
Ca	0·14	0·21	0·22	1·56	1·00	0·12	2·90	3·18	3·21	3·15	3·19	3·19
Total	16·04	16·02	16·00	16·01	16·02	15·98	16·01	16·00	15·98	15·96	15·97	16·00
Components (mol %)												
Prp	46·68	32·30	49·71	31·09	40·18	47·11	16·65	18·55	18·38	18·83	18·42	18·32
Alm	50·46	63·06	45·94	41·96	42·45	50·00	34·15	27·61	27·11	27·61	27·68	27·62
Grs	2·26	2·38	3·37	25·58	16·39	1·76	43·98	42·49	42·72	41·70	43·59	42·75
Sps	0·60	1·08	0·75	0·92	0·75	0·91	0·93	0·77	0·77	0·77	0·47	0·77
Adr	0·00	1·17	0·00	0·00	0·00	0·00	3·59	9·65	10·10	10·15	8·69	9·61
X_{Mg}	0·48	0·34	0·52	0·43	0·49	0·49	0·33	0·40	0·40	0·41	0·40	0·40

Compositions 3-17B, 20-22B, 24-33B and 40-46B are mean values, respectively, of 12, three, 10 and six tightly clustered analyses. Fe^{3+} calculated according to stoichiometry. $X_{Mg} = Mg/(Mg + Fe^{2+})$.

value of 0·42, whereas the second group clusters around 16 mol % grossular and approaches the X_{Mg} value (0·49–0·52) of the homogeneous low-Ca garnet (Fig. 3a–c).

Because of the clearly lower X_{Mg} value, we consider the most calcic core composition as part of a biotite-bearing prograde assemblage. This is consistent with the observation that biotite is included in garnet but is not involved in the peak-metamorphic assemblage. Therefore, its disappearance must have rendered garnet, as the only remaining Fe–Mg phase, more magnesian. It follows that the second group of relic garnet cores with Ca-rich and high-X_{Mg} composition may have equilibrated under peak P–T conditions. The lower grossular content of this garnet probably results from the Ca depletion of the effective bulk composition and from fractionation of Ca into coexisting ternary feldspar and, presumably, into a liquid phase.

The spinel–plagioclase coronas around garnet and kyanite show textural evidence of the CFMAS reaction Grt + Ky = Spl + Pl ± Crn, which requires grossular contents in garnet ≥83 mol %. Although this range far exceeds even the highest analysed grossular content, it may well have been reached, because the reaction occurred under strong outward diffusion of Ca in garnet. Whereas part of the garnet was consumed, the remainder was pervasively homogenized, with remarkable Ca loss.

The garnet–clinopyroxene granulite has garnet of contrasting composition, with 46–38 mol % grossular, 27–39 mol % almandine, 19–13 mol % pyrope and up to 10 mol % andradite. Marginal zoning against the symplectite assemblage is evident from depletion in Ca and Mg and enrichment in Fe^{2+} (Fig. 3d). The X_{Mg} value decreases accordingly from 0·41–0·37 in the core to 0·36–0·26 at the rims.

Table 2: Representative clinopyroxene compositions (see text for textural types)

Sample:	G97-3	G97-3	G97-3	G97-3	G97-3	G97-3	G97-3	G97-3	G97-3	G97-3	G97-3	G97-3
Analysis:	1-P	4-P	6-P	8-P	40-P	43-P	46-P	50-P	51-P	9-B	12-P	18-B
Type:	Cpx_1	Cpx_1	Cpx_1	Cpx_1	Cpx_2	Cpx_2	Cpx_2	Cpx_2	Cpx_2	Cpx_3	Cpx_3	Cpx_3
SiO_2	43·65	41·18	41·16	42·10	50·03	50·31	50·72	50·07	49·76	42·99	43·81	44·92
TiO_2	0·63	0·72	0·67	1·60	0·36	0·32	0·29	0·27	0·27	1·03	0·96	0·57
Al_2O_3	15·18	18·94	17·53	16·18	7·98	7·41	7·03	7·07	6·96	12·68	10·91	11·26
FeO^T	9·35	9·21	10·65	9·32	8·54	8·55	8·54	8·98	9·33	12·11	12·19	11·87
MnO	0·07	0·05	0·13	0·06	0·06	0·05	0·11	0·09	0·09	0·27	0·18	0·26
MgO	7·86	6·53	6·32	7·50	10·48	10·73	10·93	10·98	10·97	7·22	7·60	8·08
CaO	22·80	23·12	22·93	23·09	20·94	20·82	21·04	21·15	21·19	23·31	23·18	22·16
Na_2O	0·52	0·48	0·40	0·46	1·62	1·61	1·52	1·28	1·14	0·34	0·44	0·72
Total	100·06	100·23	99·79	100·31	100·01	99·80	100·18	99·89	99·71	99·95	99·27	99·84
Cations per 6 oxygens												
Si	1·63	1·54	1·55	1·57	1·85	1·87	1·88	1·86	1·85	1·63	1·67	1·70
Al^{iv}	0·37	0·46	0·45	0·43	0·15	0·13	0·12	0·14	0·15	0·37	0·33	0·30
Al^{vi}	0·30	0·37	0·33	0·29	0·20	0·20	0·19	0·17	0·16	0·20	0·16	0·20
Ti	0·02	0·02	0·02	0·05	0·01	0·01	0·01	0·01	0·01	0·03	0·03	0·02
Fe^{3+}	0·07	0·09	0·11	0·08	0·04	0·05	0·03	0·05	0·05	0·14	0·14	0·12
Fe^{2+}	0·22	0·20	0·23	0·21	0·23	0·22	0·23	0·23	0·24	0·25	0·25	0·25
Mn	0·00	0·00	0·01	0·00	0·00	0·00	0·00	0·00	0·00	0·01	0·01	0·01
Mg	0·44	0·36	0·36	0·42	0·58	0·59	0·60	0·61	0·61	0·41	0·43	0·45
Ca	0·91	0·92	0·93	0·93	0·83	0·83	0·83	0·84	0·85	0·95	0·95	0·90
Na	0·04	0·03	0·03	0·03	0·12	0·12	0·11	0·09	0·08	0·03	0·03	0·05
Total	4·00	3·99	4·02	4·01	4·01	4·02	4·00	4·00	4·00	4·02	4·00	4·00
Components (mol %)												
Di	38·03	31·47	30·91	35·91	50·21	51·46	52·26	51·83	51·43	37·65	40·88	39·72
Hd	19·01	17·42	19·79	17·87	19·63	19·09	19·96	19·72	20·01	22·89	23·64	22·13
Jd	3·12	2·82	2·24	2·76	9·84	9·46	9·28	7·24	6·26	1·53	1·79	3·30
CaTs	25·82	33·31	29·98	25·77	9·88	8·90	8·47	9·17	9·16	18·27	14·72	16·01
X_{Mg}	0·67	0·64	0·61	0·67	0·72	0·73	0·72	0·72	0·72	0·62	0·63	0·64

Fe^{3+} calculated according to stoichiometry.

Clinopyroxene in the garnet–clinopyroxene granulite varies in composition according to its occurrence in the sample (Fig. 4). Clinopyroxene included in garnet (Cpx_1) and clinopyroxene in symplectite (Cpx_3) have fassaitic compositions. Both are similar in jadeite content (2–4 mol %) and X_{Mg} (0·60–0·72) but vary in Ca-Tschermak component from 24–34 mol % in Cpx_1 to 13–21 mol % in Cpx_3. The matrix clinopyroxene (Cpx_2) is diopsidic and highest in jadeite content (5–10 mol %) and X_{Mg} (0·72–0·79) but lowest in Ca-Tschermak component (7–10 mol %). Zoning in this clinopyroxene is defined by a slight decrease in jadeite content at constant X_{Mg} towards the rims.

The variation in mineral composition and assemblage with changing metamorphic grade can be visualized using Robinson's (1980) projection of pyroxene composition space (Fig. 5). Textural and chemographic relations suggest that early clinopyroxene coexisted with spinel and plagioclase. At increasing pressure, clinopyroxene and plagioclase changed their compositions along $Al_2Mg_{-1}Si_{-1}$ and $NaSiCa_{-1}Al_{-1}$ exchange vectors, respectively, until the plagioclase–spinel tie-line moved across the whole-rock composition. This caused the early mineral assemblage to react to garnet, diopsidic clinopyroxene (Cpx_2) and titanite. The Ti-Tschermak component [$Ca(Fe^{2+},Mg)_{0·5}Ti_{0·5}AlSiO_6$] is significantly higher in Cpx_1 than in Cpx_2 and thus should have been the source for titanite growth. The post-peak change in clinopyroxene composition may be understood as a reversal of the prograde evolution.

Table 3: Representative feldspar compositions

Sample:	G97-1	G97-1	G97-1	G97-1	G97-1	G97-1	G97-1	G97-1	G97-1	G97-1	G97-3	G97-3
Analysis:	9A	27A	18A	4A	14A	48B	14B	16B	22B	28B	6	7
Position:	matrix	inc	inc	corona	corona	corona	mega	mega	mega	mega	sympl	sympl
SiO_2	65·05	65·77	58·85	63·69	61·27	60·58	64·44	63·81	64·28	64·80	53·74	53·32
Al_2O_3	21·92	21·33	25·52	22·76	24·48	24·57	20·15	20·30	20·25	20·14	28·75	29·12
Fe_2O_3	0·51	0·21	0·24	0·20	0·47	0·11	0·00	0·01	0·00	0·00	0·13	0·28
CaO	2·68	2·64	7·60	4·01	5·83	6·45	1·84	1·92	1·81	1·65	11·72	12·17
BaO	0·13	0·13	0·00	0·02	0·00	0·01	0·14	0·18	0·22	0·19	0·11	0·07
Na_2O	9·94	9·77	7·11	9·08	8·05	8·11	5·08	5·07	4·62	5·09	4·95	4·70
K_2O	0·16	0·39	0·33	0·25	0·27	0·22	8·40	8·25	8·94	8·58	0·03	0·03
Total	100·39	100·24	99·65	100·01	100·37	100·05	100·05	99·54	100·12	100·45	99·43	99·69
Cations per 8 oxygens												
Si	2·86	2·90	2·64	2·82	2·72	2·69	2·91	2·90	2·91	2·92	2·44	2·42
Al	1·14	1·11	1·35	1·19	1·28	1·29	1·07	1·09	1·08	1·07	1·54	1·56
Fe^{3+}	0·02	0·01	0·01	0·01	0·02	0·00	0·00	0·00	0·00	0·00	0·01	0·01
Ca	0·13	0·12	0·37	0·19	0·28	0·31	0·09	0·09	0·09	0·08	0·57	0·59
Ba	0·00	0·00	0·00	0·00	0·00	0·00	0·00	0·00	0·00	0·00	0·00	0·00
Na	0·85	0·83	0·62	0·78	0·69	0·70	0·45	0·45	0·41	0·44	0·44	0·42
K	0·01	0·02	0·02	0·01	0·02	0·01	0·48	0·48	0·52	0·49	0·00	0·00
Total	5·01	4·99	5·01	5·00	5·01	5·00	5·00	5·01	5·01	5·00	5·00	5·00
Components (mol %)												
An	13·13	12·37	36·63	19·39	28·28	30·39	8·82	8·82	8·82	7·92	56·44	58·42
Ab	85·86	85·57	61·39	79·59	69·70	68·63	44·12	44·12	40·20	43·56	43·56	41·58
Or	1·01	2·06	1·98	1·02	2·02	0·98	47·06	47·06	50·98	48·51	0·00	0·00

Inc, inclusion; mega, broad-beam analysis of megacrystic mesoperthite; sympl, symplectite.

Titanite in the garnet–clinopyroxene granulite contains 14–28 mol % fluor-titanite component [$Ca(Al,Fe^{3+})FSiO_4$] and 0–4 mol % hydroxy-titanite component [$Ca(Al,Fe^{3+})(OH)SiO_4$]. The Al_2O_3 content and X_F [F/(OH + F)] values of 0·81–1·00 are in support of high-temperature, high-pressure conditions of formation (e.g. Enami *et al.*, 1993). Fe^{3+} contributes ~10% to the (Al + Fe^{3+}) substitution for Ti (Fig. 6).

Feldspar forms several populations in both samples. Microtextural evidence supports the presence of hypersolvus ternary feldspar in the peak metamorphic assemblage of the sapphirine-bearing granulite. This feldspar now occurs as string mesoperthite, showing a fine lamellar exsolution texture with a fairly constant lamellar width of 2 μm. Broad-beam electron microprobe analysis of 24 mesoperthite megacrysts using a 50 μm beam yielded original compositions in the range of 7–11 mol % anorthite, 35–49 mol % albite and 41–56 mol % K-feldspar, with an average of 10 mol % anorthite, 44 mol % albite and 46 mol % K-feldspar. The composition varies only little, with most of the scatter being caused by three analyses (Fig. 7). The chosen beam size allowed several analyses on a single grain and clearly was large enough to reintegrate the exsolved phases. It also produced satisfactory gross stoichiometry and oxide totals. Plagioclase in the matrix of the sapphirine-bearing granulite is lowest in anorthite content (9–17 mol %). The outer corona plagioclase around garnet and kyanite shows intermediate anorthite content (18–24 mol %), and coronitic or symplectitic plagioclase in equilibrium with spinel or sapphirine has the highest anorthite content (26–33 mol %). The plagioclase inclusions in garnet are similar in composition to the matrix plagioclase or even more calcic than the inner corona plagioclase, with anorthite contents in the range of 36–57 mol %. The anorthitic inclusions are commonly irregular in shape; they probably form part of coronas randomly cut by the plane of the thin section. Although the data obtained from the garnet–clinopyroxene granulite are few, there is a clear distinction between the plagioclase rims on clinopyroxene with 38–40 mol % anorthite and symplectitic plagioclase containing 56–59 mol % anorthite.

Table 4: Representative spinel and sapphirine compositions

Sample:	G97-1	G97-1	G97-1	G97-1	G97-1	G97-1	G97-1	G97-1	G97-3	G97-1	G97-1	G97-1
Analysis:	5A	6A	13A	18A	20A	1B	13B	14B	1	3A	7B	13B
Mineral:	Spl	Spl	Spl	Spl	Spl	Spl	Spl	Spl	Spl	Spr	Spr	Spr
Position:	corona	corona	corona	corona	corona	corona	corona	corona	inc	sympl	sympl	sympl
SiO_2	0·05	0·02	0·05	0·03	0·03	0·02	0·03	0·02	0·02	12·26	12·38	13·35
TiO_2	0·03	0·03	0·03	0·05	0·03	0·04	0·04	0·04	0·00	0·07	0·09	0·08
Al_2O_3	64·39	63·94	63·38	62·54	62·43	62·80	62·74	62·20	57·75	63·52	63·34	61·71
Cr_2O_3	0·23	0·23	0·11	0·26	0·20	0·41	0·43	0·24	0·04	0·21	0·09	0·08
Fe_2O_3	0·00	0·00	0·00	0·89	1·95	0·70	1·06	1·79	5·01	1·01	0·17	1·50
FeO	21·15	21·55	25·52	24·44	22·71	19·36	19·75	23·46	30·03	7·71	9·30	6·53
ZnO	n.a.	n.a.	n.a.	0·24	0·43	3·73	2·71	0·97	0·27	0·00	0·04	0·05
MnO	0·01	0·06	0·04	0·00	0·08	0·04	0·05	0·04	0·07	0·06	0·00	0·03
MgO	13·41	12·95	10·74	11·30	12·27	12·47	12·85	11·50	7·09	14·98	14·09	16·42
Total	99·27	98·78	99·87	99·75	100·13	99·57	99·66	100·26	100·28	99·82	99·50	99·75
	Cations per 32 oxygens									*Cations per 20 oxygens*		
Si	0·01	0·00	0·01	0·00	0·00	0·00	0·00	0·00	0·00	1·47	1·49	1·59
Ti	0·00	0·00	0·00	0·01	0·00	0·01	0·01	0·01	0·00	0·01	0·01	0·01
Al	16·00	16·02	15·98	15·79	15·65	15·80	15·72	15·65	15·15	8·95	9·00	8·68
Cr	0·04	0·04	0·01	0·04	0·04	0·06	0·08	0·04	0·01	0·02	0·01	0·01
Fe^{3+}	0·00	0·00	0·00	0·14	0·31	0·11	0·17	0·29	0·84	0·09	0·02	0·14
Fe^{2+}	3·73	3·83	4·56	4·37	4·04	3·45	3·51	4·19	5·59	0·77	0·94	0·65
Zn	0·00	0·00	0·00	0·04	0·06	0·59	0·42	0·15	0·04	0·00	0·00	0·01
Mn	0·00	0·01	0·01	0·00	0·01	0·01	0·01	0·01	0·01	0·01	0·00	0·00
Mg	4·22	4·10	3·42	3·60	3·88	3·96	4·08	3·66	2·35	2·67	2·54	2·92
Total	24·00	24·00	23·99	23·99	23·99	23·99	24·00	24·00	23·99	13·99	14·01	14·01
X_{Mg}	0·53	0·52	0·43	0·45	0·49	0·53	0·54	0·47	0·30	0·78	0·73	0·82

Partitioning of ferrous/ferric iron in spinel by charge balance, and in sapphirine according to Higgins *et al.* (1979). n.a., not analysed.

Spinel compositions from both rocks fall mainly in the solid solution series $FeAl_2O_4$–$MgAl_2O_4$, with Cr_2O_3 contents generally below 0·5 wt % and only traces of TiO_2 and MnO. The coronitic spinel in the sapphirine-bearing granulite varies in X_{Mg} between 0·40–0·47 on kyanite and 0·48–0·54 on garnet. It contains up to 3·7 wt % ZnO and <2 wt % Fe_2O_3. Spinel included in garnet of the garnet–clinopyroxene granulite is characterized by an X_{Mg} value of 0·30, traces of ZnO, and Fe_2O_3 contents of ~5 wt %.

Sapphirine in the sapphirine-bearing granulite has Al_2O_3 contents equal to or a little lower than the 7:9:3 composition (Fig. 8). Ferric estimates employing the method of Higgins *et al.* (1979) yield Fe_2O_3 contents of 0·2–1·5 wt %. The contents of TiO_2, Cr_2O_3, ZnO and MnO are low or negligible. Like spinel, sapphirine in contact with kyanite is lower in X_{Mg} (0·73–0·77) than sapphirine in contact with garnet (0·75–0·82).

Biotite from the sapphirine-bearing granulite forms two textural types that differ in composition. Biotite included in garnet has 6·6–7·4 wt % TiO_2 and X_{Mg} values of 0·74–0·75. Secondary biotite is lower in TiO_2 (1·6–4·1 wt %) but higher in X_{Mg} (0·79–0·80). Both types are similar with respect to Al_2O_3 (15·3–16·8 wt %) and F (0·2–0·7 wt %). Biotite included in garnet is enriched in Cl (0·2–0·3 wt %) and BaO (0·3–0·5 wt %) compared with the secondary biotite.

Amphibole in symplectite of the garnet–clinopyroxene granulite invariably is pargasite. As oxidizing conditions are evident in this rock, the formula calculation has been based on maximum ferric estimates. Mean ferric formulae, if used instead, would still correspond to pargasite according to the IMA 97 scheme (Leake *et al.*, 1997). The Si content varies from 5·8 to 6·0 p.f.u., and the X_{Mg} value from 0·59 to 0·67. The halogen content is high, comprising 1·7–2·5 wt % F and 0·2–0·6 wt % Cl. Pargasite or magnesiohastingsite with lower X_{Mg} (0·51–0·55) occurs within fractures that cut across the compositional layering in the rock.

Magnetite in symplectite of the garnet–clinopyroxene

Table 5: Representative biotite and amphibole compositions

Sample:	G97-1	G97-1	G97-1	G97-1	G97-1	G97-1	G97-3	G97-3	G97-3	G97-3	G97-3	G97-3
Analysis:	1A	4A	8A	9A	13A	15A	1	2	3	4	6	7
Mineral:	Bt	Bt	Bt	Bt	Bt	Bt	Am	Am	Am	Am	Am	Am
Position:	crack	inc	inc	inc	inc	inc	sympl	sympl	sympl	sympl	sympl	sympl
SiO_2	38·60	37·61	36·57	37·19	36·96	37·08	38·56	39·02	38·80	39·79	39·90	39·51
TiO_2	4·13	6·51	6·87	6·79	6·87	6·36	0·96	0·85	0·82	0·90	1·14	1·11
Al_2O_3	16·81	15·49	15·83	15·77	15·64	16·33	16·17	15·31	16·12	15·79	15·12	15·27
Cr_2O_3	0·13	0·01	0·04	0·02	0·03	0·02	0·00	0·00	0·00	0·00	0·00	0·00
FeO^T	8·32	10·30	9·83	10·05	10·08	9·72	16·08	15·75	15·79	13·90	14·57	14·65
MnO	0·04	0·00	0·00	0·00	0·02	0·02	0·25	0·23	0·18	0·16	0·18	0·15
MgO	18·19	16·16	16·37	16·14	16·08	16·27	9·63	9·98	9·78	10·99	10·95	10·82
CaO	0·00	0·00	0·00	0·00	0·00	0·00	11·83	11·97	11·76	11·75	11·90	12·07
BaO	0·08	0·26	0·41	0·45	0·31	0·27	0·00	0·00	0·00	0·00	0·00	0·00
Na_2O	0·21	0·24	0·33	0·32	0·32	0·13	3·10	3·13	3·14	3·34	3·29	3·48
K_2O	8·90	8·97	9·19	9·08	9·05	9·39	0·30	0·28	0·32	0·17	0·12	0·11
F	0·33	0·32	0·61	0·65	0·50	0·27	2·27	2·49	2·46	2·18	2·19	1·69
Cl	0·13	0·21	0·21	0·17	0·17	0·22	0·55	0·51	0·58	0·18	0·17	0·16
Total	95·70	95·90	95·96	96·32	95·78	95·92	98·62	98·36	98·58	98·19	98·57	98·27
	Cations per 22 oxygens						*Cations per 23 oxygens*					
Si	5·53	5·48	5·34	5·41	5·40	5·39	5·80	5·90	5·84	5·93	5·94	5·92
Al^{iv}	2·47	2·52	2·66	2·59	2·60	2·61	2·20	2·10	2·16	2·07	2·06	2·08
Al^{vi}	0·37	0·14	0·07	0·11	0·10	0·19	0·67	0·63	0·70	0·71	0·60	0·62
Ti	0·45	0·71	0·75	0·74	0·76	0·70	0·11	0·10	0·09	0·10	0·13	0·13
Cr	0·02	0·00	0·01	0·00	0·00	0·00	0·00	0·00	0·00	0·00	0·00	0·00
Fe^{3+}	0·00	0·00	0·00	0·00	0·00	0·00	0·53	0·42	0·49	0·40	0·42	0·33
Fe^{2+}	1·00	1·25	1·20	1·22	1·23	1·18	1·49	1·57	1·50	1·33	1·40	1·50
Mn	0·01	0·00	0·00	0·00	0·00	0·00	0·04	0·03	0·03	0·02	0·03	0·02
Mg	3·89	3·51	3·56	3·50	3·50	3·53	2·16	2·25	2·20	2·45	2·43	2·41
Ca	0·00	0·00	0·00	0·00	0·00	0·00	1·91	1·94	1·90	1·88	1·90	1·93
Ba	0·01	0·02	0·03	0·03	0·02	0·02	0·00	0·00	0·00	0·00	0·00	0·00
Na	0·06	0·07	0·10	0·09	0·09	0·04	0·90	0·92	0·91	0·97	0·95	1·01
K	1·63	1·66	1·71	1·69	1·69	1·74	0·05	0·06	0·06	0·04	0·03	0·02
Total	15·44	15·36	15·43	15·38	15·39	15·40	15·86	15·92	15·88	15·90	15·89	15·97
X_{Mg}	0·80	0·74	0·75	0·74	0·74	0·75	0·59	0·59	0·59	0·65	0·64	0·62

Oxide total corrected for the oxygen weight-equivalent of F and Cl. Allocation of total Fe assuming all-ferrous formulae for biotite and maximum ferric formulae for amphibole (all cations exclusive of Ca, Na, K = 13).

granulite is composed of 66–73 mol % magnetite, 18–23 mol % ulvöspinel and 6–10 mol % hercynite.

Muscovite overgrowths on plagioclase in the garnet–clinopyroxene granulite are low in Si (3·06–3·15 p.f.u.) and have negligible Na_2O content.

P–T evolution

If not stated otherwise, the *P–T* data in the following section were computed using Berman's (1991) TWQ program, version 2·02, with the site allocation and preferred solution models, and the thermodynamic database (Berman & Aranovich, 1996) contained therein.

Sapphirine-bearing granulite (G97-1)

Textural and mineral chemical evidence for the presence of a single ternary feldspar phase generally implies that either the consolute point on a two-feldspar isotherm or hypersolvus conditions were attained. As the ternary

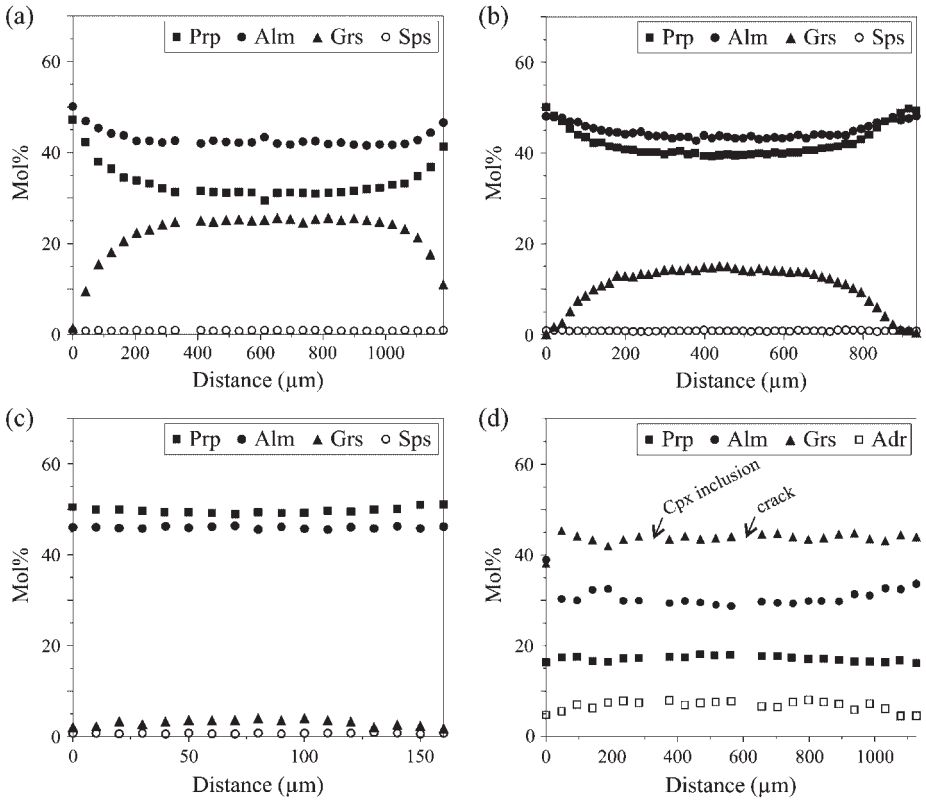

Fig. 3. Garnet composition profiles. (a–c) Sapphirine-bearing granulite (G97-1): (a) strongly zoned garnet with Ca-rich and relatively low-X_{Mg} (0·42) core; (b) zoned garnet with Ca-rich and high-X_{Mg} (0·48) core; (c) homogenized Ca-poor and high-X_{Mg} (0·52) garnet similar in composition to the rims of zoned garnet crystals. (d) Garnet–clinopyroxene granulite (G97-3): marginally zoned almandine–grossular garnet with andradite component.

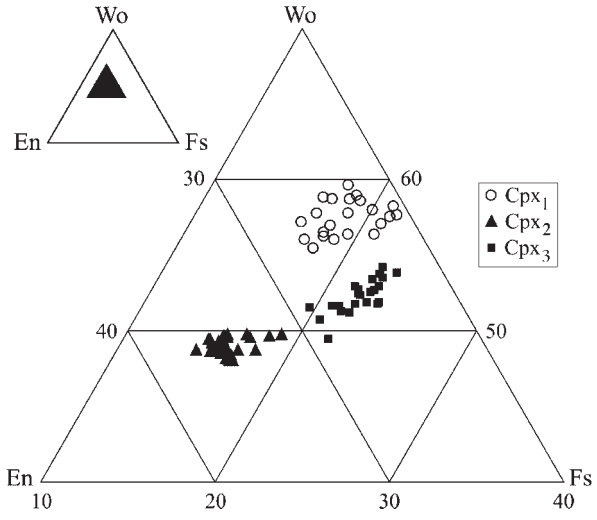

Fig. 4. Section of the wollastonite–enstatite–ferrosilite ternary illustrating the compositional variation of clinopyroxene in the garnet–clinopyroxene granulite (G97-3). The inset shows the position of the enlarged section.

feldspar solvus is little dependent on pressure, the occurrence of ternary feldspar similar in composition to the consolute point on a two-feldspar isotherm suggests, for reasonable estimates of pressure, that the temperature was close to this isotherm. If the composition of a single ternary feldspar phase is away from any relevant consolute point, only a minimum temperature can be estimated. In any case, estimating temperature from mesoperthite requires a reliable estimate of the original, unexsolved feldspar composition. On the basis of a feldspar solution model, this composition can then be used to calculate the composition of the companion feldspar that falls on the opposite limb of the same two-feldspar isotherm. In practice, this is done by trial and error, calculating two-feldspar temperatures from the reintegrated ternary feldspar and from a hypothetical feldspar whose composition is changed in a stepwise fashion until all three temperatures obtained from the components of both feldspars show a close match.

By employing this method, Rötzler *et al.* (1998) obtained minimum temperatures for felsic granulites in the SGM in the range of 945–1015°C at 22 kbar. On an isotherm diagram the reintegrated ternary feldspar compositions

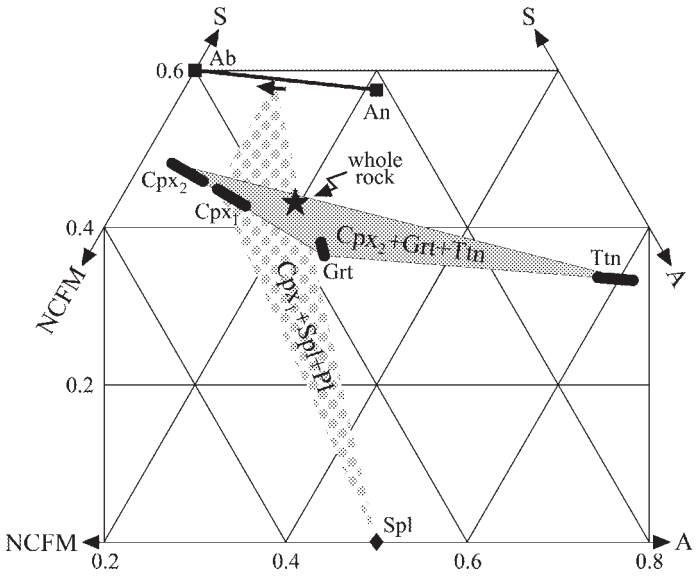

Fig. 5. Section of the S–NCFM–A ternary diagram after Robinson (1980) showing the topology of successive mineral assemblages in the garnet–clinopyroxene granulite (G97-3). S is SiO_2; NCFM is 2 Na_2O + CaO + FeO + MnO + MgO – TiO_2; A is Al_2O_3 + Fe_2O_3 + Cr_2O_3 + 2 TiO_2 – Na_2O (on a molecular basis). Whole-rock data are from Rötzler (unpublished). (See text for explanation.)

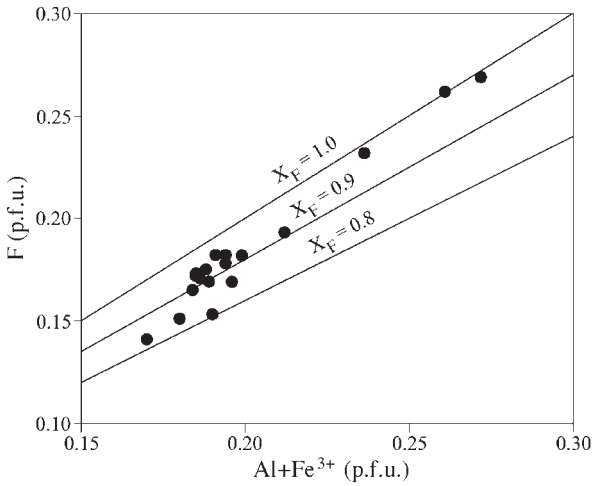

Fig. 6. Fluorine vs Al + Fe^{3+} for titanite in the garnet–clinopyroxene granulite (G97-3). X_F = F/(OH + F).

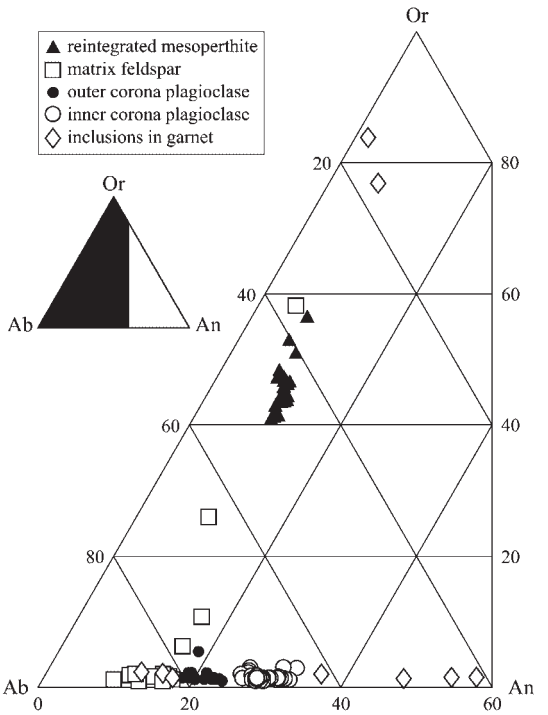

Fig. 7. Variation of feldspar composition in the sapphirine-bearing granulite (G97-1). The inset shows the position of the enlarged section of the Or–Ab–An ternary diagram.

reported here from the sapphirine-bearing granulite plot near or above the solvus at 900°C and 22 kbar (Fig. 9). For these compositions, the trial-and-error approach using the model of Fuhrman & Lindsley (1988) yields minimum temperature estimates in the range of 935–984°C, assuming a pressure of 22 kbar, with an average of 967 ± 12°C (1σ).

Peak pressure estimates were extracted from the GASP reaction between ternary feldspar and garnet. For the reasons discussed above, it seems valid to assume that the peak-metamorphic garnet is preserved in relic cores, linking Ca-rich with high-X_{Mg} composition. Hence, the evaluation was based on the average of these tightly clustered core compositions (24-33B in Table 1) and on the individual compositions of 24 ternary feldspars. The resulting pressure estimates are in the range of

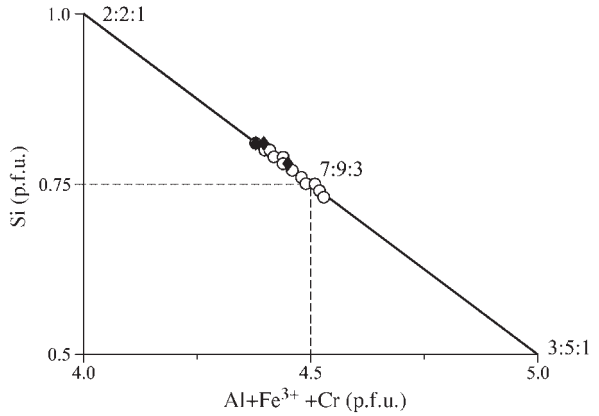

Fig. 8. Si vs Al + Fe^{3+} + Cr for sapphirine of the sapphirine-bearing granulite (G97-1; ○) and of the kornerupine-bearing granulite at Waldheim (after Grew, 1986; ◆). The bold line denotes the solid solution series (Mg, Fe^{2+})$^{vi}Si^{iv}$ = (Al, Fe^{3+},Cr)$^{vi}Al^{iv}$, with various RO: R_2O_3:SiO_2 members indicated.

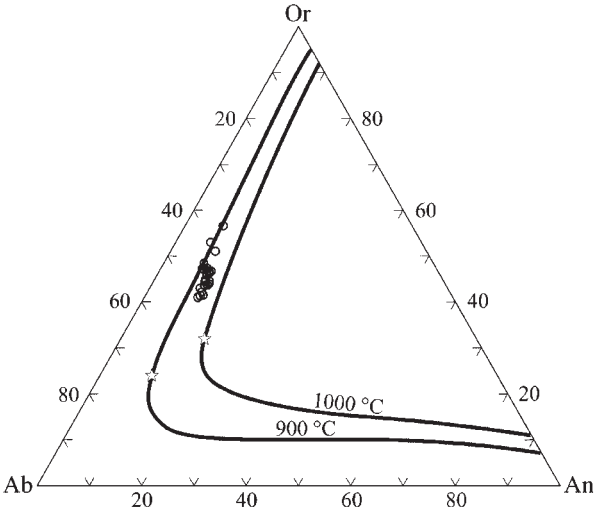

Fig. 9. Reintegrated ternary feldspar compositions (○) from the sapphirine-bearing granulite (G97-1), plotted in relation to the feldspar isotherms and consolute points (open stars) at 900°C and 1000°C, 22 kbar according to the model of Fuhrman & Lindsley (1988).

21·2–23·1 kbar at 967°C, with average and 1σ uncertainty of 22·3 ± 0·4 kbar.

The breakdown of biotite in the sapphirine-bearing granulite raised the X_{Mg} value of garnet. In the fluid-absent KFMASH system, biotite melting at pressures >9 kbar occurs around 900°C (Carrington & Harley, 1995). Mouri *et al.* (1996) have argued that incorporation of fluorine into biotite may raise the onset of biotite melting to higher than 950°C. According to experiments of Patiño Douce & Johnston (1991), biotite with 5·38 wt % TiO_2 and 1·29 wt % F is stable at 975°C and 10 kbar. The biotite included in garnet of the sapphirine-bearing granulite has higher TiO_2 but lower F contents, implying that matrix biotite of similar composition should have stably persisted to a temperature clearly above 900°C. The temperature range in which fluid-absent biotite melting occurs widens with decreasing bulk X_{Mg} and increasing pressure (Carrington & Harley, 1995). The range should have been fairly wide in the sapphirine-bearing granulite, because the bulk X_{Mg} is relatively low (0·48), and high-pressure conditions are indicated by the mineral inclusion assemblage in garnet. Biotite would thus have coexisted with melt up temperature over a large melting interval, and garnet and feldspar would have simultaneously changed their compositions. Therefore, combining the Ca-rich pre-peak garnet with peak-metamorphic ternary feldspar would give erroneous GASP pressure estimates (higher by 2 kbar than the pressure range given above). As biotite dehydration melting is expected to have taken place, it is somewhat surprising that there is no corresponding textural evidence. However, such evidence may have been obscured during the ubiquitous post-peak high-temperature mylonitization.

The peak-metamorphic assemblage and *P–T* estimates of the sapphirine-bearing granulite compare with high-pressure, high-temperature experimental phase relations in a fluid-absent granitic composition (Green & Lambert, 1965), although in contrast to the experiments, no clinopyroxene formed, but kyanite was produced as a result of peraluminous bulk chemistry. The experiments show that, at 950°C, garnet replaces orthopyroxene as the pressure increases across the range of ~16 kbar. Above that, and up to ~23 kbar, the stable assemblage consists of garnet, clinopyroxene, plagioclase, alkali feldspar and quartz. On further pressure increase, plagioclase disappears and clinopyroxene grows rapidly, adopting a jadeitic composition. The phase relations at 1100°C differ from the above mainly in that hypersolvus ternary feldspar is present. The orthopyroxene breakdown and the growth of jadeitic clinopyroxene both are shifted up pressure by ~2 kbar. At the quartz–coesite transition, alkali feldspar with albite as a major component is stable over the temperature range of the experiments.

The mass-transfer reaction Grt + Ky = Spl + Pl and the garnet–spinel Fe^{2+}–Mg exchange reaction were examined to evaluate the coronitic assemblage of the sapphirine-bearing granulite. However, it is not easy to determine the equilibrium compositions for this assemblage, because on the one hand the coronitic plagioclase began to grow before the spinel-forming reaction and partly recrystallized thereafter. On the other hand, spinel may have re-equilibrated with garnet or sapphirine. The most consistent data come from spinel–plagioclase aggregates penetrating into garnet but having no contact with sapphirine. These aggregates and the adjacent garnet vary little in composition, with X_{Mg} values of 0·48–0·49 in garnet, 0·52–0·54 in spinel and 28–32 mol % anorthite in plagioclase. The end-member reactions in the CFMAS

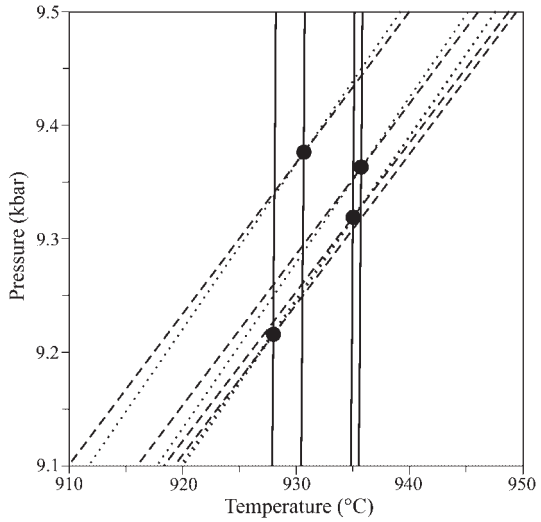

Fig. 10. *P–T* diagram showing the calculated reaction equilibria for the spinel–plagioclase coronas surrounding garnet and kyanite in the sapphirine-bearing granulite (G97-1). The reactions are: Alm + 3 Spl = Prp + 3 Hc (continuous curve), 5 Grs + Prp + 12 Ky = 3 Spl + 15 An (dashed curve) and 5 Grs + Alm + 12 Ky = 3 Hc + 15 An (dotted curve), with the product assemblages being stable on the high-temperature side of the curves. Analyses 15A, 14A and 6A in Tables 1, 3 and 4, respectively, are representative compositions used for calculation.

system calculated from these data intersect at 930–940°C and 9·2–9·4 kbar (Fig. 10).

Garnet and biotite in mutual contact will at least partially re-equilibrate on cooling as long as Fe^{2+} and Mg can diffuse across the grain boundary. The closure temperature for this diffusional exchange depends on the cooling rate, on the presence of a fluid phase and on crystal defects. Hence, the garnet–biotite thermometer applied to biotite inclusions in garnet and to biotite overgrowths on garnet in the sapphirine-bearing granulite may provide the temperature at which these mineral pairs ceased to re-equilibrate. The pressure range for the cooling path of the Saxon granulites can best be deduced from the structurally overlying units, which were successively heated during the extensional unroofing of the Granulite Complex (Kroner, 1995). The thermal peak and post-peak history of these units (Rötzler, 1992) agrees with evidence from fluid inclusions and from andalusite-bearing hydrous mineral assemblages in the granulites (Grew, 1986), indicating medium- to low-pressure conditions. Assuming a pressure of 3 kbar, host garnet and biotite inclusions in the sapphirine-bearing granulite yield temperature estimates near 740°C. In contrast, garnet rims and overgrown biotite record a temperature of 650°C for an assumed pressure of 2 kbar. As these temperature estimates are barely pressure-sensitive, they imply that the late-stage fluid infiltration into the granulites allowed diffusion within the matrix of these rocks to extend to significantly lower temperature.

Garnet–clinopyroxene granulite (G97-3)

The peak assemblage of the garnet–clinopyroxene granulite is unfavourable for barometric analysis, as plagioclase and quartz are absent, but temperature is well constrained, because the garnet–clinopyroxene Fe^{2+}–Mg exchange reaction provides a fairly pressure-insensitive thermometer. This thermometer, however, is sensitive to uncertainty in the X_{Mg} value of garnet and clinopyroxene. Because Fe^{3+} was not analysed directly, estimation was made from stoichiometric assumptions. The Fe^{3+} content in garnet was first estimated on a 24-oxygen basis by adding Fe^{3+} to bring the sum of octahedral and tetrahedral cations to 10. Alternatively, a 16-cation basis was used and Fe^{3+} was added to fit the oxygen sum to 24. The estimation of Fe^{3+} in clinopyroxene was based on six oxygen atoms, assuming that the non-quadrilateral substitutions are balanced by an adequate amount of Fe^{3+}. Another set of estimates was obtained using Berman's (1991) TWQ program. Different ferric estimates derived in this way from the same mineral analysis reflect small analytical errors, which have some effect on the thermometric evaluation. Peak temperature estimates were made from garnet and matrix clinopyroxene (Cpx_2), using core compositions of garnet high in X_{Mg}, and of clinopyroxene low in X_{Mg} but high in jadeite content. Taking into account the uncertainty in X_{Mg}, the garnet–clinopyroxene thermometer of Berman *et al.* (1995) yields a range in temperature of 1014–1062°C, assuming a pressure of 22 kbar. The uncertainty introduced by various ferric estimates is of the order of 20°C. Unlike the feldspar solvus temperatures for the sapphirine-bearing granulite (G97-1), which place only a lower limit on the thermal peak, the garnet–clinopyroxene equilibration temperatures indicate real peak conditions.

Temperature estimates for the symplectite assemblage were based on re-equilibrated garnet rims in contact with symplectitic clinopyroxene (Cpx_3). The X_{Mg} values in the garnet used for calculation range from 0·27 to 0·32; those in the clinopyroxene vary between 0·64 and 0·68. The above-described methods for computing Fe^{3+} contents and temperature yield estimates of 890–940°C, assuming a pressure of 9 kbar. These pressure-insensitive results overlap with the temperature estimates for the pressure-dependent corona assemblage of the sapphirine-bearing granulite (G97-1), implying that the pressure was of the order of 9 kbar.

A direct pressure evaluation for the symplectite of the garnet–clinopyroxene granulite is prevented by the lack of quartz and by the overstepping of the equilibrium with garnet and clinopyroxene as a result of continuous amphibole–plagioclase re-equilibration. The latter is evident from amphibole–plagioclase temperatures calculated using the edenite–richterite thermometer of Holland & Blundy (1994). These temperatures average 840

± 14°C at 9 kbar. Calculation at 4 kbar yields 794 ± 14°C (1σ), consistent with earlier *P–T* estimates, indicating cooling of the granulites through 800°C at ~4 kbar (Grew, 1986; Rötzler, 1992). Because of evidence for high-f_{O_2} conditions, the amphibole–plagioclase temperatures were estimated using maximum ferric formulae for amphibole. If mean ferric formulae were used instead, the temperatures would be lower by ~50°C.

DISCUSSION

In spite of partial re-equilibration during near-isothermal decompression from ultrahigh-temperature high-pressure conditions, peak metamorphism and post-peak evolution of the Saxon granulites can still be retrieved. Hence, our results may contribute to dispel doubts raised by Petrakakis (1997), who suspected that peak *P–T* estimates similar to those reported here, obtained from granulite occurrences elsewhere in the Bohemian Massif, are due to disequilibrium or misinterpretation of textures.

The studied rocks, two felsic granulites and one mafic granulite, have the following textures in common: (1) prograde inclusion assemblages in garnet; (2) peak assemblages in varying states of preservation; (3) multistage corona and symplectite assemblages; (4) late-stage hydrous minerals. Feldspar thermometry and GASP barometry applied to the felsic granulite indicate minimum peak *P–T* conditions of 967°C and 22·3 kbar. The mafic granulite yields peak thermal estimates of 1014–1062°C, but pressures cannot be constrained.

Rötzler *et al.* (1994) reported *P–T* estimates of 1050°C and 20 kbar from a multi-equilibrium calculation based on inclusions of plagioclase and clinopyroxene in garnet from a quartz-free mafic granulite. Reassessment of this assemblage using the TWQ program and the database from Berman & Aranovich (1996) indicates equilibration around 1060°C and 22·3 kbar. Separate calculation of the reactions Alm + 3 Di = Prp + 3 Hd and 3 An + 3 Di + 3 Jd = Prp + 2 Grs + 3 Ab employing the garnet–clinopyroxene thermometer from Berman *et al.* (1995) and the TWQ program results in estimates around 1005°C and 21·4 kbar. In summary, these data and those obtained from the samples studied here argue for a peak metamorphism of the Saxon granulites in the range of 1010–1060°C and 22 kbar.

Various corona and symplectite textures and partial re-equilibration of peak minerals are evidence of a near-isothermal exhumation of the studied rocks to less than half of their maximum depth. Symplectite of clinopyroxene + amphibole + plagioclase + magnetite from the mafic granulite formed slightly above 900°C at an inferred pressure of ~9 kbar. Garnet and kyanite of the felsic granulite are surrounded by composite corona and symplectite textures that show successive growth of (1) plagioclase, (2) spinel + plagioclase ± corundum and (3) sapphirine + plagioclase. Grew (1986, 1989), in investigating two other localities for sapphirine in the SGM, found similar textures, but also montmorillonite rims on garnet, which he interpreted as alteration products of cordierite. For this reason, Grew (1989) considered it likely that sapphirine was produced by the reaction Grt + Ky = Spr + Crd. In contrast, the felsic granulite studied here displays good evidence for the spinel-forming reaction Grt + Ky = Spl + Pl ± Crn and for subsequent formation of sapphirine by the reaction Grt + Ky + Spl = Spr + Pl. The spinel-bearing assemblage yields *P–T* estimates of 930–940°C and 9·2–9·4 kbar.

The tectonic juxtaposition of the rising granulites with middle- and upper-crustal units induced prograde metamorphism in the latter. This permits pressure estimates obtained from the structurally upper units (Rötzler, 1992) to be used to constrain the cooling path of the granulites. A mean temperature of 794°C at an assumed pressure of 4 kbar is recorded by amphibole–plagioclase equilibria in the mafic granulite. In the felsic granulite, inclusions of primary biotite in garnet consistently indicate an equilibration temperature of 740°C at an assumed pressure of 3 kbar. A much lower temperature of 650°C was derived from biotite overgrowth on garnet, assuming a pressure of 2 kbar. Both estimates are seen as the closure temperature for the retrograde Fe–Mg exchange between garnet and biotite, with the estimate for the biotite overgrowth on garnet reflecting the shift of this exchange to lower temperature in the presence of a fluid phase. The final retrograde stage is evident in local muscovite and chlorite overgrowths.

The *P–T* estimates presented here (Table 6) agree favourably with mineral equilibrium conditions and oxygen-isotope temperatures reported from granulites elsewhere in the SGM (Rötzler *et al.*, 1994, 1998; Hagen *et al.*, 1995). The depicted evolution (Fig. 11) should thus apply to the entire granulitic rock association and, in conjunction with structural, geochemical and geophysical data, allows us to make inferences about the tectonothermal and fluid regime. The peak *P–T* conditions and the lack of thermal relaxation of the Saxon granulites during uplift require a short-lived metamorphism. This follows on the one hand from physical experiments showing that deeply subducted upper continental crust can separate from the subducting plate and rise once its strength is outbalanced by buoyancy forces (Chemenda *et al.*, 1995). On the other hand, the near-isothermal decompression of the Saxon granulites and heating in the medium- to low-pressure envelope are evidence of rapid exhumation without cooling to a steady-state geotherm. As the Saxon granulites bear no indications of polymetamorphism, a short-lived event is also implied by the preservation of successive mineral assemblages, in

Table 6: Compilation of P–T *estimates (see text for explanation)*

Mineral assemblage	Felsic granulite (G97-1)	Mafic granulite (G97-3)
Peak assemblage	(1) $T \geq 967 \pm 12$°C at 22 kbar	(6) $T = 1014$–1062°C at 22 kbar
	(2) $P = 22{\cdot}3 \pm 0{\cdot}4$ kbar at 967°C	
Corona–symplectite assemblage	(3) $T = 930$–940°C, $P = 9{\cdot}2$–$9{\cdot}4$ kbar	(7) $T = 890$–940°C at 9 kbar
Amphibole–plagioclase equilibria		(8) $T = 794 \pm 14$°C at 4 kbar
Re-equilibrated biotite within garnet	(4) $T = 735$–745°C at 3 kbar	
Secondary biotite on garnet	(5) $T = 653$°C at 2 kbar	

Numbers in parentheses refer to symbols in Fig. 11.

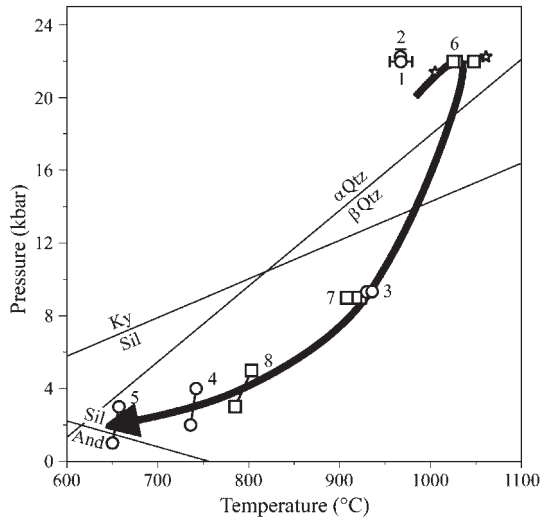

Fig. 11. Summary *P–T* diagram for the metamorphic evolution in the Saxon Granulite Complex. Numbers next to symbols refer to the *P–T* estimates listed in Table 6. Open stars indicate additional *P–T* estimates for host garnet and inclusions of clinopyroxene and plagioclase from a mafic granulite, recalculated after Rötzler *et al.* (1994) using the methods discussed in the text.

particular of prograde mineral relics. Experiments on the solubility of Al in pyroxenes performed at high pressure in the CMAS system (e.g. Nickel *et al.*, 1985) produced Al contents similar to those analysed in the clinopyroxene inclusions (Cpx_1) in the mafic granulite only at significantly higher temperature than the thermal peak inferred for the Saxon granulites. This discrepancy may result from the more complex composition of our natural sample compared with the simple system experiments, or may indicate that the clinopyroxene inclusions formed originally under igneous conditions, in contrast to the previously suggested calc-silicate protolith of this rock (Werner, 1987).

Direct magmatic heating as a potential cause of ultrahigh-temperature metamorphism does not apply to the SGM, as syn-granulitic magmatic intrusions are absent. Purely conductive heating by imbricate thrusting of thin slivers of subcrustal rocks may have occurred, although the volume proportion of such rocks exposed at the surface is insufficient, and there is also no positive gravity anomaly in the area of the SGM (Conrad, 1996) to suggest the presence of ultramafic–mafic rocks in the subsurface. The absence of hydrous minerals and of melt reactions in the peak assemblages of the Saxon granulites indicates very low volatile activity. This is in line with the lack of a pronounced depletion of large-ion lithophile elements (Rötzler, 1992). Hence advective heating of the Saxon granulites by fluids is unlikely and the heat source of the metamorphism remains speculative.

Among several geotectonic models invoked recently by the DEKORP Working Group (1999), only one (specified B4 by that group) can be reconciled with the new data presented by Jaeckel *et al.* (1999) and Romer & Rötzler (2001). This model assumes southerly dipping subduction zones in Late Devonian and Early Carboniferous times between the lithospheric plates (Rheno-Hercynian, Saxo-Thuringian and Tepla-Barrandian terranes) that collided to form the Central European Variscan belt. The protoliths of the Saxon granulites are thought to originate either from the Saxo-Thuringian terrane or the plate margin of the Tepla-Barrandian terrane to the south. The southward subduction of the granulite protoliths beneath the Tepla-Barrandian terrane and their return to the Saxo-Thuringian upper crust are explainable by a mechanism similar to that proposed by Chemenda *et al.* (1995), including southeasterly extensional unroofing of the rising Granulite Complex (Kroner, 1995). Dating of the peak metamorphism of the granulites at 342 Ma (Romer & Rötzler, 2001) and of granitoid intrusions into the exhumed granulites at 333 Ma (Nasdala *et al.*, 1996;

Kröner *et al.*, 1998) limits the time span for the exhumation of the Saxon granulites to ~9 my.

ACKNOWLEDGEMENTS

Electron microprobe analysis at Potsdam was assisted by O. Appelt and W. Seifert. H. Kemnitz helped with the scanning electron microscopy. Thanks also go to M. Dziggel for drawing the final version of the geological map. Travel funding for this study was provided by the German Research Council (DFG) through grant KE 552/2-3. The original manuscript benefited from constructive reviews by L. Kriegsman, R. Kryza and an anonymous reviewer.

REFERENCES

Baumann, N., Pilot, J., Werner, C.-D. & Todt, W. (1997). On the geochronology and isotope geochemistry of the Saxon Granulite Massif (in German). *Terra Nostra* **97**(5), 19–22.

Berman, R. G. (1991). Thermobarometry using multiequilibrium calculations: a new technique with petrologic applications. *Canadian Mineralogist* **29**, 833–855.

Berman, R. G. & Aranovich, L. Ya. (1996). Optimized standard state and solution properties of minerals; I, Model calibration for olivine, orthopyroxene, cordierite, garnet, and ilmenite in the system FeO–MgO–CaO–Al_2O_3–TiO_2–SiO_2. *Contributions to Mineralogy and Petrology* **126**, 1–24.

Berman, R. G., Aranovich, L. Ya. & Pattison, D. R. M. (1995). Reassessment of the garnet–clinopyroxene Fe–Mg exchange thermometer: II. Thermodynamic analysis. *Contributions to Mineralogy and Petrology* **119**, 30–42.

Carrington, D. P. & Harley, S. L. (1995). Partial melting and phase relations in high-grade metapelites: an experimental petrogenetic grid in the KFMASH system. *Contributions to Mineralogy and Petrology* **120**, 270–291.

Chemenda, A. I., Mattauer, M., Malavieille, J. & Bokun, A. N. (1995). A mechanism for syn-collisional rock exhumation and associated normal faulting: results from physical modelling. *Earth and Planetary Science Letters* **132**, 225–232.

Conrad, W. (1996). The gravity map of Brandenburg, Mecklenburg–Western Pomerania, Saxony, Saxony–Anhalt and Thuringia: remarks and interpretation (in German). *Sächsisches Landesamt für Boden und Geologie, Geoprofil* **6**, 1–56.

DEKORP Working Group (1999). Structure of the Saxonian Granulites: geological and geophysical constraints on the exhumation of high-pressure/high-temperature rocks in the mid-European Variscan belt. *Tectonics* **18**, 756–773.

Enami, M., Suzuki, K., Liou, J. G. & Bird, D. K. (1993). $Al–Fe^{3+}$ and F–OH substitutions in titanite and constraints on their *P–T* dependence. *European Journal of Mineralogy* **5**, 219–231.

Fuhrman, M. L. & Lindsley, D. H. (1988). Ternary-feldspar modeling and thermometry. *American Mineralogist* **73**, 201–215.

Gaitzsch, B. G. (1998). Flysch and early molasse deposits in the eastern Saxo-Thuringian zone and in the Saxo-Lugicum (in German). *Terra Nostra* **98**(2), 49–52.

Green, D. H. & Lambert, I. B. (1965). Experimental crystallization of anhydrous granite at high pressures and temperatures. *Journal of Geophysical Research* **70**, 5259–5268.

Grew, E. S. (1986). Petrogenesis of kornerupine at Waldheim (Sachsen), German Democratic Republic. *Zeitschrift für Geologische Wissenschaften* **14**, 525–558.

Grew, E. S. (1989). A second occurrence of kornerupine in Waldheim, Saxony, German Democratic Republic. *Zeitschrift für Geologische Wissenschaften* **17**, 67–76.

Hagen, B. (1994). Thermometry and geochemistry on rocks from the Saxon Granulite Massif (in German). Diploma thesis, University of Bonn, 69 pp.

Hagen, B., Hoernes, S. & Rötzler, J. (1995). Consistent ultra-high temperatures in the Saxonian granulite massif as deduced from cation exchange and O-isotope thermometry. *Terra Abstracts* **7**, 340.

Higgins, J. B., Ribbe, P. H. & Herd, R. K. (1979). Sapphirine I. Crystal chemical contributions. *Contributions to Mineralogy and Petrology* **68**, 349–356.

Holland, T. & Blundy, J. (1994). Non-ideal interactions in calcic amphiboles and their bearing on amphibole–plagioclase thermometry. *Contributions to Mineralogy and Petrology* **116**, 433–447.

Jaeckel, P., Anthes, G., Molzahn, M., Oncken, O. & Reischmann, T. (1999). Pb isotopic systematics of the Central Variscan belt. *Terra Nostra* **99**(1), 111–112.

Kröner, A., Jaeckel, P., Reischmann, T. & Kroner, U. (1998). Further evidence for an early Carboniferous (~340 Ma) age of high-grade metamorphism in the Saxonian granulite complex. *Geologische Rundschau* **86**, 751–766.

Kroner, U. (1995). Post-collisional extension at the northern margin of the Bohemian Massif: the exhumation of the Saxon Granulite Massif (in German). *Freiberger Forschungshefte* **C457**, 1–114.

Kryza, R., Pin, C. & Vielzeuf, D. (1996). High-pressure granulites from the Sudetes (south-west Poland): evidence of crustal subduction and collisional thickening in the Variscan belt. *Journal of Metamorphic Geology* **14**, 531–546.

Leake, B. E. and 21 others (1997). Nomenclature of amphiboles: report of the Subcommittee on Amphiboles of the International Mineralogical Association, Commission on New Minerals and Mineral Names. *American Mineralogist* **82**, 1019–1037.

Mouri, H., Guiraud, M. & Hensen, B. J. (1996). Petrology of phlogopite–sapphirine-bearing Al–Mg granulites from Ihouhaouene, In Ouzzal, Hoggar, Algeria: an example of phlogopite stability at high temperature. *Journal of Metamorphic Geology* **14**, 725–738.

Nasdala, L., Gruner, T., Nemchin, A. A., Pidgeon, R. T. & Tichomirowa, M. (1996). New SHRIMP ion microprobe measurements on zircons from Saxonian magmatic and metamorphic rocks. *Proceedings of the Freiberg Isotope Colloquium*. Freiberg University of Mining and Technology, pp. 205–214.

Nickel, K. G., Brey, G. P. & Kogarko, L. (1985). Orthopyroxene–clinopyroxene equilibria in the system CaO–MgO–Al_2O_3–SiO_2 (CMAS): new experimental results and implications for two-pyroxene thermometry. *Contributions to Mineralogy and Petrology* **91**, 44–53.

Patiño Douce, A. E. & Johnston, A. D. (1991). Phase equilibria and melt productivity in the pelitic system: implications for the origin of peraluminous granitoids and aluminous granulites. *Contributions to Mineralogy and Petrology* **107**, 202–218.

Petrakakis, K. (1997). Evolution of Moldanubian rocks in Austria: review and synthesis. *Journal of Metamorphic Geology* **15**, 203–222.

Pin, C. & Vielzeuf, D. (1983). Granulites and related rocks in Variscan median Europe: a dualistic interpretation. *Tectonophysics* **93**, 47–74.

Rauche, H. (1994). Kinematics and timing of the ductile to brittle transition in mylonites from the Elbe Zone–Erzgebirge border shear zone (Mid-Saxonian fault, eastern Saxothuringian). *Journal of the Czech Geological Society* **39**, 88–89.

Robinson, P. (1980). The composition space of terrestrial pyroxenes—internal and external limits. In: Prewitt, C. T. (ed.) *Pyroxenes. Mineralogical Society of America, Reviews in Mineralogy* **7**, 419–494.

Romer, R. L. & Rötzler, J. (2001). *P–T–t* evolution of ultrahigh-temperature granulites from the Saxon Granulite Massif, Germany. Part II: Geochronology. *Journal of Petrology* **42**, 2015–2032.

Rötzler, J. (1992). On the petrogenesis in the Saxon Granulite Massif (in German, with English abstract). *Geotektonische Forschungen* **77**, 1–100.

Rötzler, J., Budzinski, H. & Budzinski, G. (1994). Evidence for Early Variscan very high temperature (>1000°C)–high pressure metamorphism of garnet–clinopyroxene granulites in the Saxon Granulite Massif, Germany. *European Journal of Mineralogy* **6**, Supplement 1, 234.

Rötzler, J., Hagen, B. & Hoernes, S. (1998). Ultrahigh-temperature high-pressure metamorphism in the Saxon Granulite Massif, Germany. *Terra Nostra* **98**(2), 130–131.

Rötzler, J., Carswell, D. A., Gerstenberger, H. & Haase, G. (1999). Transitional blueschist–epidote amphibolite facies metamorphism in the Frankenberg Massif, Germany, and geotectonic implications. *Journal of Metamorphic Geology* **17**, 109–125.

Vavra, G. & Reinhardt, J. (1997). Which processes are dated by U/Pb zircon ages of high-grade metamorphic rocks? Zircon genesis in various lithologies and structural levels of the Saxonian Granulite Massif. *Terra Nostra* **97**(5), 190–192.

Vavra, G., Reinhardt, J., Todt, W. & Pidgeon, R. T. (1998). Dating of exhumation of a hot core complex (Saxonian Granulite Massif)—old prejudices and new perspectives of U–Pb dating of zircons and monazite. *Freiberger Forschungshefte* **C471**, 226–228.

von Quadt, A. (1993). The Saxonian Granulite massif: new aspects from geochronological studies. *Geologische Rundschau* **82**, 516–530.

Werner, C.-D. (1987). Saxonian granulites: a contribution to the geochemical diagnosis of original rocks in high-metamorphic complexes. *Gerlands Beiträge zur Geophysik* **96**, 271–290.

Werner, O. & Reich, S. (1997). $^{40}Ar/^{39}Ar$ cooling ages for rocks with different *P–T* evolution from the Schist Cover of the Saxon Granulite Massif (in German). *Terra Nostra* **97**(5), 196–198.